

Full-waveform inversion of multicomponent data for horizontally layered VTI media

Nishant Kamath¹ and Ilya Tsvankin¹

ABSTRACT

Although full-waveform inversion (FWI) has shown significant promise in reconstructing heterogeneous velocity fields, most existing methodologies are limited to acoustic models. We extend FWI to multicomponent (PP and PS) data from anisotropic media, with the current implementation limited to a stack of horizontal, homogeneous VTI (transversely isotropic with a vertical symmetry axis) layers. The algorithm is designed to estimate the interval vertical P- and S-wave velocities (V_{P0} and V_{S0}) and Thomsen parameters ϵ and δ from long-spread PP and PSV reflections. The forward-modeling operator is based on the anisotropic reflectivity technique, and the inversion is performed in the time domain using the gradient (Gauss-Newton) method. We employ nonhyperbolic semblance analysis and Dix-type equations to build the initial model. To identify the medium parameters constrained by the data, we perform eigenvalue/eigenvector

decomposition of the approximate Hessian matrix for a VTI layer embedded between isotropic media. Analysis of the eigenvectors shows that the parameters V_{P0} , V_{S0} , ϵ , and δ (density is assumed to be known) can be resolved not only by joint inversion of PP and PS data, but also with PP reflections alone. Although the inversion becomes more stable with increasing spreadlength-to-depth (X/Z) ratio, the parameters of the three-layer model are constrained even by PP data acquired on conventional spreads ($X/Z = 1$). For multilayered VTI media, the sensitivity of the objective function to the interval parameters decreases with depth. Still, it is possible to resolve V_{P0} , V_{S0} , ϵ , and δ for the deeper layers using PP-waves, if the ratio X/Z for the bottom of the layer reaches two. Mode-converted waves provide useful additional constraints for FWI, which become essential for smaller spreads. The insights gained here by examining horizontally layered models should help guide the inversion for heterogeneous TI media.

INTRODUCTION

Transversely isotropic media with a vertical axis of symmetry (VTI) can be described by the vertical P- and S-wave velocities, V_{P0} and V_{S0} , and the Thomsen parameters ϵ , δ , and γ . However, traveltimes analysis of PP-wave reflection data typically yields just the P-wave normal-moveout velocity $V_{\text{nmo},P}$ and anellipticity coefficient η (Alkhalifah and Tsvankin, 1995).

Tsvankin and Thomsen (1995) show that all four parameters of horizontally layered VTI media responsible for propagation of P- and SV-waves (V_{P0} , V_{S0} , ϵ , and δ) can be obtained from long-spread PP- and SS (SVSV)-wave traveltimes. Shear waves, however, are not excited in offshore surveys, and their quality on land is often unsatisfactory. Therefore, here we consider joint

inversion of PP-waves and converted PSV modes (hereafter, denoted by PS; there is no P-to-SH conversion in laterally homogeneous VTI media). The replacement of pure SS reflections with PS-waves, however, complicates velocity analysis because even long-spread traveltimes of PP- and PS-waves are insufficient for constraining the interval parameters V_{P0} , V_{S0} , ϵ , and δ of layer-cake VTI models (Grechka and Tsvankin, 2002).

Here, we examine the feasibility of reconstructing stratified VTI models in depth using full-waveform inversion (FWI) of PP and PS data. FWI can be performed either in the time domain (Gauthier, 1986; Kolb et al., 1986; Mora, 1987; Bunks et al., 1995) or frequency domain (Song and Williamson, 1995; Song et al., 1995; Pratt, 1999; Pratt and Shipp, 1999). It is typically based on gradient estimation by zero-lag crosscorrelation of the source and residual

Manuscript received by the Editor 28 September 2012; revised manuscript received 5 April 2013; published online 25 July 2013; corrected version published online 17 September 2013.

¹Colorado School of Mines, Center for Wave Phenomena, Golden, Colorado, USA. E-mail: nkamath@mines.edu; ilya@dix.mines.edu.

© 2013 Society of Exploration Geophysicists. All rights reserved.

receiver wavefields, as described in [Tarantola \(1984\)](#). Most existing algorithms are designed for isotropic, acoustic media, and they operate primarily with diving waves. Numerical experiments performed by [Lee et al. \(2010\)](#) show that isotropic FWI applied to anisotropic models gives unsatisfactory results. In order to extend FWI to anisotropic media, it is highly beneficial to combine PP-wave data with PS- or SS-waves, which requires using elastic models. Taking elasticity into account also makes it possible to properly model reflection amplitudes and take advantage of matching the entire waveform rather than just phase information.

[Plessix and Rynja \(2010\)](#) implement FWI for VTI media in the acoustic approximation to invert for $V_{\text{nm},P}$, η , and δ . [Lee et al. \(2010\)](#) estimate the stiffness coefficients of 2D VTI media by frequency-domain elastic FWI of multicomponent data and conclude that it is difficult to obtain good estimates of the coefficient C_{13} . Parameterization in terms of the stiffnesses, however, is not optimal for inversion purposes ([Tsvankin, 2012](#)) and creates trade-offs that can be avoided by using [Thomsen \(1986\)](#) notation. Single- and multiparameter acoustic FWI for VTI media are performed by [Gholami et al. \(2011\)](#). In the former case, they estimate only one velocity (V_{P0} , $V_{\text{nm},P}$, or the horizontal velocity $V_{\text{hor},P}$), while the long-wavelength variations of ϵ and δ are fixed at the correct values. They also invert for two velocities ($V_{\text{hor},P}$ and V_{P0}) under the assumption that the long-wavelength spatial variation of δ is known. [Gholami et al. \(2011\)](#) demonstrate that the single-parameter inversion provides a good estimate of the unknown velocity, while multiparameter inversion suffers from nonuniqueness. [Plessix and Cao \(2011\)](#) implement acoustic FWI for diving waves and near-offset reflections to reconstruct the long-wavelength components of the P-wave NMO and horizontal velocities in VTI media.

[Chang and McMechan \(2009\)](#) present a feasibility study of FWI for a horizontal anisotropic layer sandwiched between isotropic media. In addition to TI layers with a vertical (VTI) and horizontal (HTI) symmetry axis, they also consider a layer of orthorhombic symmetry. They use multicomponent data to invert for the vertical P- and S-wave velocities, anisotropy parameters, and density of the anisotropic layer as well as for the parameters of the underlying isotropic half-space. They conclude that wide-azimuth reflections from the top and bottom of the anisotropic layer are needed for stable interval parameter estimation.

Here, we develop an FWI algorithm for multicomponent data from horizontally layered VTI media. PP and PS reflections from all interfaces are inverted simultaneously, which mitigates downward error propagation through the model. First, we describe application of moveout inversion to building the initial model from just PP-wave moveout or from the combination of PP and PS reflection traveltimes. Then we analyze the Hessian matrix for layered VTI models to identify the parameters constrained by input data acquired for a realistic range of spreadlength-to-depth (X/Z) ratios. Finally, the inversion algorithm is applied separately to PP data alone and to the combination of PP and PS reflections to evaluate the feasibility of building VTI depth models from different sets of input data.

METHODOLOGY

We model PP- and PS (PSV)-waves excited by a point explosive source with the anisotropic reflectivity method ([Mallick and Frazer, 1990](#)) using a Ricker wavelet with a peak frequency of 15 Hz. The data include free-surface multiples, but direct arrivals are not mod-

eled. In practice, reflection data are sorted into common-midpoint gathers to minimize reflection-point dispersal. However, here, FWI operates on a single shot gather because the medium is horizontally layered. Both the horizontal and vertical displacement components are used for inverting PP-waves and the combination of PP and PS data. The algorithm is tested for different spreadlengths with the receiver spacing kept constant at 25 m. The parameters of the first layer (or the overburden) are assumed to be known and are fixed at the correct values during the inversion.

Building the initial model

To obtain the initial model, we employ widely used moveout-inversion techniques. Time processing of PP reflection data in VTI media is fully controlled by the parameters $V_{\text{nm},P}$ and η , which can be estimated from PP-wave traveltimes:

$$V_{\text{nm},P} = V_{P0} \sqrt{1 + 2\delta}, \quad (1)$$

$$\eta = \frac{\epsilon - \delta}{1 + 2\delta}. \quad (2)$$

The long-spread reflection moveout of PP-waves in a horizontal VTI layer is well described by the nonhyperbolic equation of [Alkhalifah and Tsvankin \(1995\)](#):

$$t^2 = t_{P0}^2 + \frac{x^2}{V_{\text{nm},P}^2} - \frac{2\eta x^4}{V_{\text{nm},P}^2 [t_{P0}^2 V_{\text{nm},P}^2 + (1 + 2\eta)x^2]}, \quad (3)$$

where x is the offset and t_{P0} is the two-way zero-offset time. The velocity $V_{\text{nm},P}$ controls the moveout on conventional spreads, while η is responsible for deviation from hyperbolic moveout in long-spread data. In moveout inversion, the parameter η is often replaced with the P-wave horizontal velocity $V_{\text{hor},P} = V_{\text{nm},P} \sqrt{1 + 2\eta}$.

Equation 3 remains valid for layered VTI media, with $V_{\text{nm},P}$ and η becoming effective quantities for the stack of layers above the reflector. For spreadlength-to-depth ratios X/Z reaching 1.5–2, equation 3 can be used to perform 2D semblance scanning and estimate the effective parameters $V_{\text{nm},P}$ and η ([Grechka and Tsvankin, 1998](#)). Then the interval velocity $V_{\text{nm},P}$ is found from the conventional Dix equation and the interval η from the Dix-type equation given in [Grechka and Tsvankin \(1998\)](#) and [Tsvankin \(2012\)](#). If the offset range is wide enough to record head waves, the interval $V_{\text{hor},P}$ can be estimated directly from the head-wave moveout ([Tsvankin, 2012](#)).

The initial value of δ is set to zero, which allows us to find the parameters V_{P0} and ϵ from $V_{\text{nm},P}$ and η . The density ρ and shear-wave vertical velocity V_{S0} (if only PP data are available) for the initial model are supposed to be found from well logs. Potentially, the accuracy of the initial model can be improved by using velocity-independent layer stripping ([Wang and Tsvankin, 2009](#)).

For multicomponent data, it is necessary to identify the PP and PS (PSV) reflections from the same interfaces (i.e., perform event registration). The interval values of $V_{\text{nm},P}$ and η can be calculated from P-wave data as described above. To estimate the effective PS-wave NMO velocity ($V_{\text{nm},PS}$), we apply a 2D semblance scan based on equation 3 to long-spread PS data. In this case, η

represents just a fitting parameter, but the equation is sufficiently accurate to constrain $V_{\text{nmo,PS}}$, which replaces $V_{\text{nmo,P}}$ (Xu and Tsvankin, 2008). Then the effective NMO velocity $V_{\text{nmo,SV}}$ of the pure SS reflection can be found from (Seriff and Sriram, 1991)

$$2 t_{\text{PS0}} V_{\text{nmo,PS}}^2 = t_{\text{P0}} V_{\text{nmo,P}}^2 + t_{\text{S0}} V_{\text{nmo,SV}}^2, \quad (4)$$

where t_{PS0} and t_{S0} are the zero-offset traveltimes of PS- and SS-waves, respectively, so that $t_{\text{S0}} = 2t_{\text{PS0}} - t_{\text{P0}}$. The interval SV-wave NMO velocity, obtained from the Dix equation, is given by

$$V_{\text{nmo,SV}} = V_{\text{S0}} \sqrt{1 + 2\sigma}, \quad (5)$$

where $\sigma \equiv (V_{\text{P0}}/V_{\text{S0}})^2(\varepsilon - \delta)$.

In principle, all four parameters (V_{P0} , V_{S0} , ε , and δ) can be found from $V_{\text{nmo,P}}$, $V_{\text{nmo,SV}}$, $V_{\text{P0}}/V_{\text{S0}} = t_{\text{S0}}/t_{\text{P0}}$, and η . Although this procedure is known to be unstable (Grechka and Tsvankin, 2002), it provides us with an acceptable initial model for FWI.

Inversion algorithm

We perform time-domain inversion of either PP data alone or the combination of PP and PS reflections. The least-squares objective function is defined as

$$\mathcal{F}(\mathbf{m}) = \frac{1}{2} \|\mathbf{d}_{\text{obs}} - \mathbf{d}_{\text{cal}}(\mathbf{m})\|^2, \quad (6)$$

where \mathbf{d}_{obs} is the observed data and $\mathbf{d}_{\text{cal}}(\mathbf{m})$ is the data calculated for a certain model \mathbf{m} . Model updating is carried out via the Gauss-Newton method,

$$\Delta \mathbf{m} = [\mathbf{J}^T \mathbf{J}]^{-1} \mathbf{J}^T \Delta \mathbf{d}, \quad (7)$$

where \mathbf{J} is the Fréchet derivative matrix obtained by perturbing each model parameter, $\mathbf{J}^T \mathbf{J}$ is the approximate Hessian, and $\Delta \mathbf{d}$ is the difference between the observed data and those computed for a trial model. Forward modeling is carried out with the anisotropic reflectivity algorithm of Mallick and Frazer (1990) mentioned above, based on the formulation introduced by Fryer and Frazer (1984). The main advantage of that method is that it produces the exact 3D reflected wavefield for horizontally layered media including all multiples and mode conversions. In addition, it is possible to separate the wavefield and model either just PP reflections or PP and mode-converted PS data.

Because the vertical velocities and anisotropy parameters do not have the same units, it is more convenient to invert PP data for the interval parameters V_{P0} , $V_{\text{nmo,P}}$, $V_{\text{hor,P}}$, $V_{\text{P0}}/V_{\text{S0}}$, and the density ρ . In the case of joint inversion of PP and PS data, we estimate the interval values of V_{P0} , $V_{\text{nmo,P}}$, V_{S0} , $V_{\text{nmo,SV}}$, and ρ . The initial values of V_{P0} and V_{S0} obtained from PP and PS data can be used to calculate the initial $V_{\text{P0}}/V_{\text{S0}}$ ratio for the inversion of PP-waves. If only PP reflections are acquired, the initial $V_{\text{P0}}/V_{\text{S0}}$ has to be known a priori (e.g., from well logs).

INVERSION RESULTS

Model 1

First, the FWI algorithm is applied to the simple three-layer model in Figure 1. The top layer is isotropic, and its velocities

and density are assumed to be known. The bottom half-space is also known to be isotropic, but its parameters are estimated by FWI.

We perform tests for data with the spreadlength-to-depth ratio X/Z ranging from one to three. For $X/Z = 1$, the parameter η cannot be constrained by PP reflection traveltimes, so the initial values of ε and δ are set to zero. For larger spreads ($X/Z = 1.5, 2, \text{ and } 3$), inversion is performed with the initial parameters computed from moveout inversion as described above.

The testing shows that the interval parameters V_{P0} , V_{S0} , ε , and δ can be constrained by FWI, but the inversion is highly sensitive to the starting model when the data include PP and PS reflections. When PP and PS data are inverted jointly with the initial $\delta = 0$, the algorithm converges to the correct values only for $X/Z = 1$. For longer spreads, accurate inversion requires calculating the initial δ from moveout inversion, even though errors in δ can reach 0.6. This is likely due to the shape of the objective function, which causes the inversion for the initial $\delta = 0$ to get trapped in local minima. As discussed below, this problem can be mitigated by applying a multiscale approach.

To evaluate the sensitivity of the objective function to the model parameters, we perform the eigenvector/eigenvalue decomposition of the Hessian matrix (Plessix and Cao, 2011) for joint inversion of PP and PS data. Each component of an eigenvector (called the “direction cosine” and represented by the circles in Figure 2b) indicates the relative sensitivity of the objective function to one of the model parameters. The gradient of the objective function is a linear combination of the eigenvectors weighted by the eigenvalues of the Hessian (Figure 2a).

Figure 2b displays the eigenvectors associated with the four largest eigenvalues. It shows that the objective function is most sensitive to the layer thickness D (and hence to V_{P0} because the vertical traveltimes are well constrained), followed by V_{S0} , $V_{\text{nmo,P}}$, and $V_{\text{nmo,SV}}$.

All our tests demonstrate that the objective function becomes more complicated with the inclusion of density as an unknown parameter, and the search gets trapped in local minima. In spite of the relatively low sensitivity of the objective function to density (Figure 2b), performing inversion with densities distorted by up to 10% results in unacceptable errors in all inverted parameters. In particular, the velocity V_{P0} and layer thicknesses are off by about 5%.

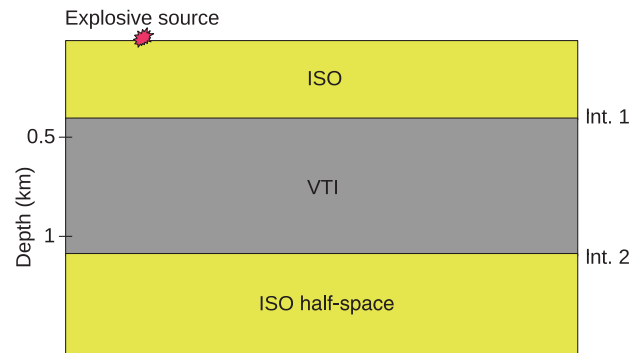


Figure 1. Three-layer model used in the tests. The parameters of the top isotropic layer are $V_{\text{P}} = 2800$ m/s, $V_{\text{S}} = 1400$ m/s, and $\rho = 1.8$ g/cm³. For the VTI layer, $V_{\text{P0}} = 3000$ m/s, $V_{\text{S0}} = 1632$ m/s, $\varepsilon = 0.25$, $\delta = 0.1$, and $\rho = 2.4$ g/cm³. For the bottom half-space, $V_{\text{P}} = 3400$ m/s, $V_{\text{S}} = 1800$ m/s, and $\rho = 3.2$ g/cm³. Interfaces (“Int.”) are numbered from top to bottom.

Hence, in all subsequent tests, the interval densities are fixed at the correct values. In practice, densities are often estimated from well-log data, whereas in synthetic tests of FWI, they are typically fixed at a constant value (e.g., Lee et al., 2010). In principle, density can be better constrained using global optimization techniques such as genetic algorithms (Padhi and Mallick, 2013). For realistic models with a large number of parameters, however, global optimization is extremely expensive.

Next, we generate only PP data for the same model and invert for the parameters V_{P0} , $V_{nmo,P}$, $V_{hor,P}$, and V_{P0}/V_{S0} . For all spread-lengths X/Z , the algorithm converges to the correct parameters, even though the initial value of δ is set to zero. Evidently, the objective function has a simpler shape with fewer local minima, if only PP data are included.

Interestingly, the inversion yields accurate parameter estimates even for $X/Z = 1$ despite the absence of PS data (Figure 3a). This is an unexpected result, especially because such spreadlengths are not sufficient to constrain even the horizontal velocity (or the parameter η) and, therefore, ε using reflection traveltimes. The data misfit, normalized by the value at the first iteration, is shown in Figure 3b. Apparently, the success of FWI is ensured by including reflection amplitudes controlled by geometric spreading and reflection coefficient.

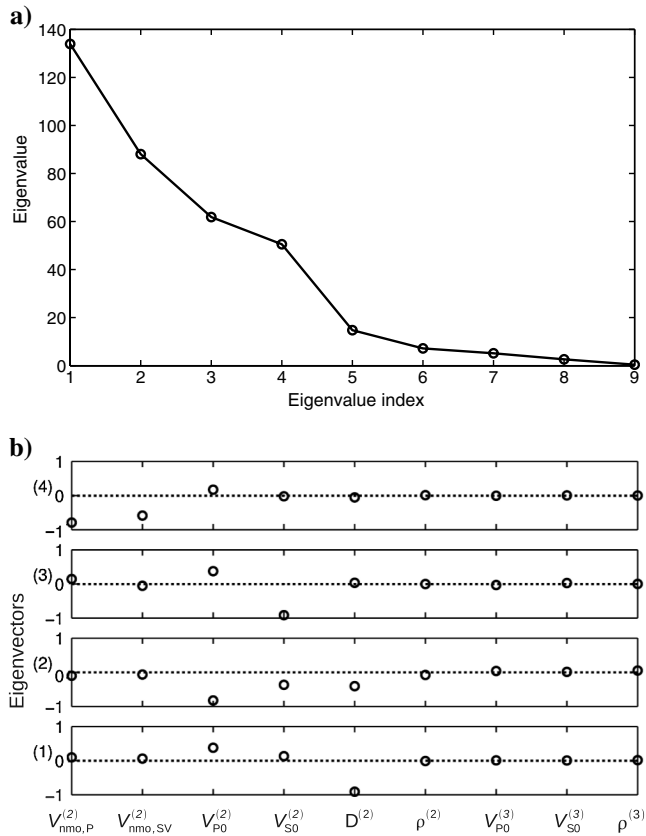


Figure 2. (a) Eigenvalues of the Hessian matrix. (b) Components of the eigenvectors (numbered 1 to 4) associated with the four largest eigenvalues of the Hessian. The input data include PP and PS reflections for the model in Figure 1 for $X/Z = 1.5$. The superscript (2) denotes the VTI layer and (3) the bottom isotropic half-space. The thickness of the VTI layer is denoted by D .

Indeed, angle dependence of the far-field amplitude of P-waves excited by a point explosive source in a homogeneous, weakly anisotropic TI medium can be written as (Tsvankin, 1995, 2012; Xu et al., 2005)

$$A_P(\theta) \sim 1 - 2(\varepsilon - \delta) \sin^2 2\theta + \delta \sin^2 \theta, \quad (8)$$

where θ is the phase angle with the symmetry axis. For small angles θ , the amplitude variation (i.e., the anisotropic geometric spreading) is largely controlled by $\eta \approx \varepsilon - \delta$. Although equation 8 is derived for a homogeneous medium, it also describes the behavior of the anisotropic geometric-spreading factor in any TI layer crossed by the reflected ray (Tsvankin, 2012).

The PP-wave reflection coefficient at a boundary between two VTI half-spaces in the weak-contrast, weak-anisotropy ($|\delta| \ll 1$, $|\varepsilon| \ll 1$) approximation is given by (Rüger, 1997, 2002)

$$R = \frac{1}{2} \frac{\Delta Z}{Z} + \frac{1}{2} \left[\frac{\Delta V_{P0}}{V_{P0}} - \left(\frac{2\bar{V}_{S0}}{V_{P0}} \right)^2 \frac{\Delta G}{G} + \Delta\delta \right] \sin^2 \theta + \frac{1}{2} \left[\frac{\Delta V_{P0}}{V_{P0}} + \Delta\varepsilon \right] \sin^2 \theta \tan^2 \theta, \quad (9)$$

where θ is the incidence phase angle, $Z = \rho V_{P0}$ is the P-wave vertical impedance, and $G = \rho V_{S0}^2$ is the S-wave vertical rigidity

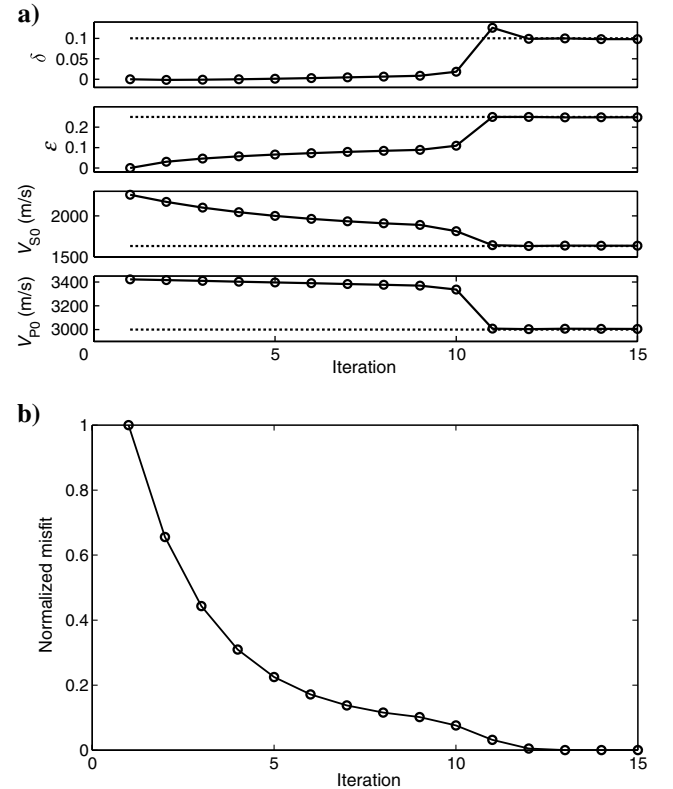


Figure 3. (a) Parameters of the VTI layer (circles) after each iteration of FWI; the actual values are marked by the horizontal dashed lines. The input data include PP reflections for the model in Figure 1 for $X/Z = 1$. (b) Data misfit computed from equation 6 and normalized by the value for the initial model.

modulus. The difference between each parameter B (V_{P0} , V_{S0} , etc.) below and above the reflector is denoted by $\Delta B = B_2 - B_1$, and the average is $\bar{B} = (B_1 + B_2)/2$. The first term in equation 9 is the normal-incidence reflection coefficient, also known as the AVO intercept, which is equal to the fractional difference between the P-wave impedances in the two media. The second term is responsible for amplitude variation near the vertical and is called the AVO gradient. It depends on the relative change in V_{P0} and G across the interface and on the contrast in the parameter δ . Hence, PP-wave reflection amplitudes at small offsets are sensitive to the jumps in V_{P0} , V_{S0} , ρ , and δ .

Because the densities in all layers and the velocities in the shallowest layer are fixed at the correct values, the amplitude signatures help resolve all VTI parameters for the model in Figure 1. In particular, the normal-incidence reflection coefficient provides constraints on V_{P0} in the VTI layer and the bottom half-space, whereas amplitude variation with angle helps us estimate the other parameters. Note that the P-wave AVO gradient (and the P-wave reflection coefficient as a whole) includes the jump in the vertical rigidity modulus G (equation 9), which creates a dependence of the FWI objective function on V_{S0} . Still, the objective function for PP-wave inversion is not as sensitive to the V_{P0}/V_{S0} ratio as it is to V_{P0} and D (Figure 4), partially because the exact P-wave geometric-spreading factor in the $0^\circ - 40^\circ$ range typically changes

by less than 2%–3% for the V_{P0}/V_{S0} ratio varying from 1.73 to 2.2 (Tsvankin, 2012). We conclude that FWI of PP reflections can reconstruct the depth scale of this three-layer model even without using long-offset data.

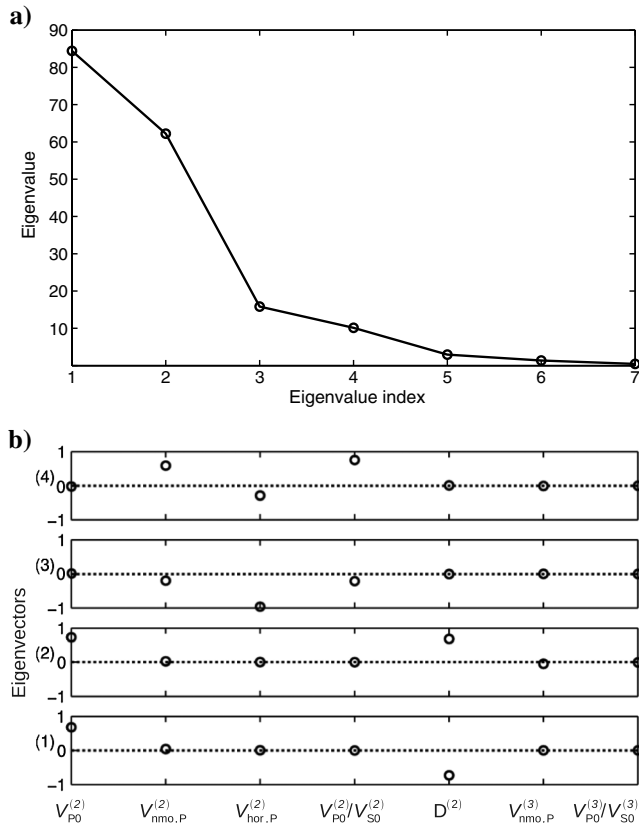


Figure 4. (a) Eigenvalues of the Hessian matrix and (b) the components of the eigenvectors (numbered 1 to 4) associated with the four largest eigenvalues of the Hessian. The input data include PP reflections for the model in Figure 1 for $X/Z = 1$.

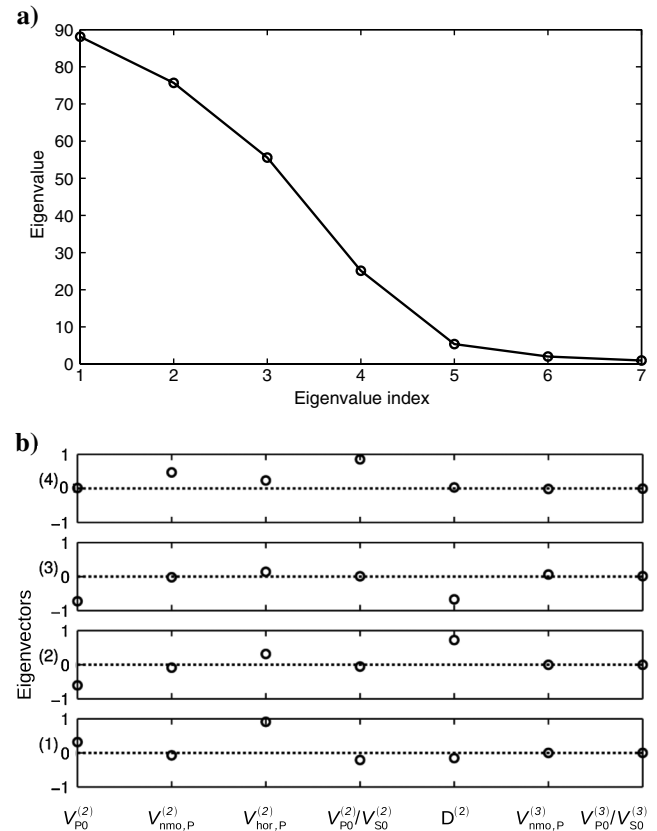


Figure 5. (a) Eigenvalues of the Hessian matrix and (b) the components of the eigenvectors (numbered 1 to 4) associated with the four largest eigenvalues of the Hessian. The input data include PP reflections for the model in Figure 1 for $X/Z = 2$. The data are contaminated with band-limited (10–25 Hz) random noise; the signal-to-noise ratio is five.

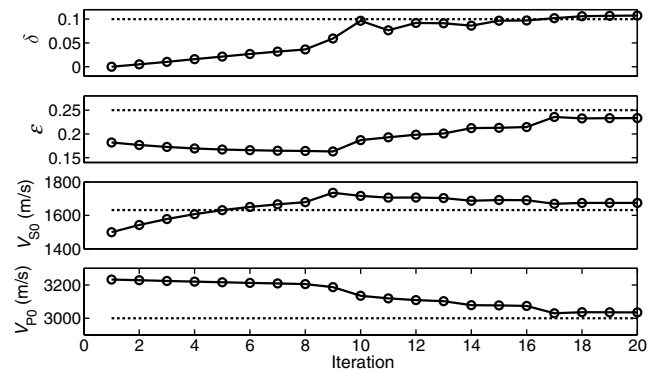


Figure 6. Parameters of the VTI layer (circles) after each iteration of FWI. The input data include PP reflections for the model in Figure 1 for $X/Z = 2$. The data are contaminated with band-limited (10–25 Hz) random noise; the signal-to-noise ratio is five.

When larger offsets are included, the velocity $V_{hor,P}$ (or η) is well resolved even in the presence of random noise because it governs the magnitude of nonhyperbolic moveout. Indeed, for $X/Z = 2$, the

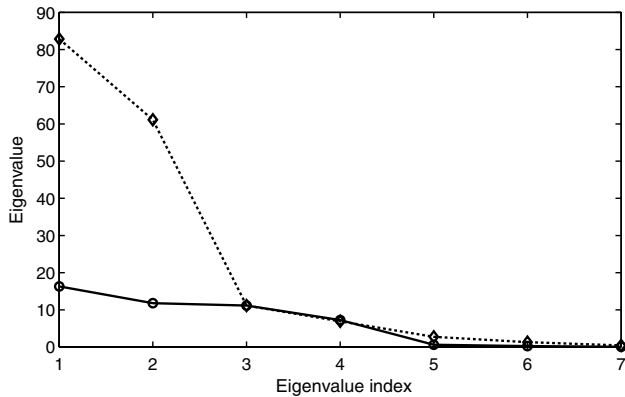


Figure 7. Eigenvalues of the Hessian matrices associated with the horizontal displacement component (circles) and the vertical component (diamonds). The input data include PP reflections for the model in Figure 1 for $X/Z = 1$.

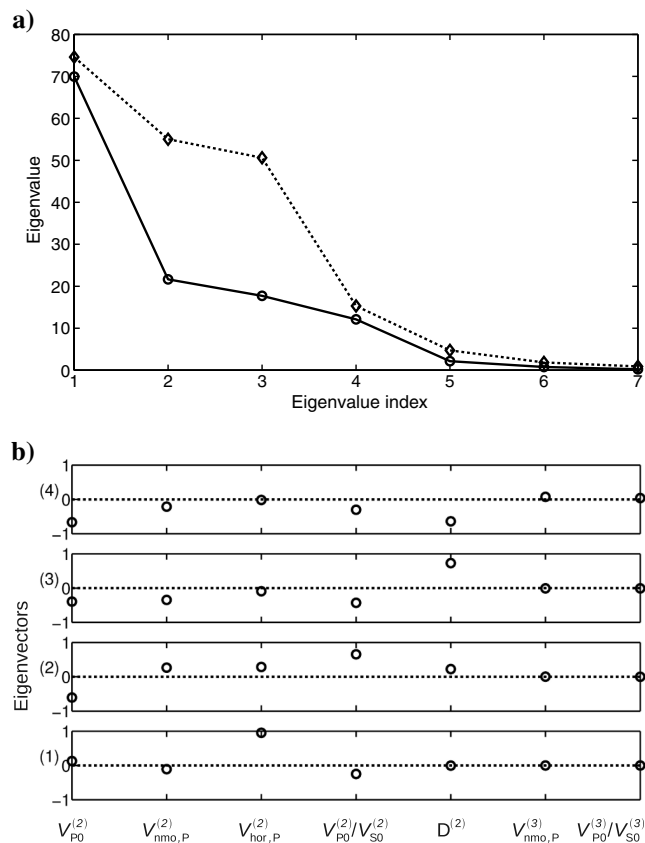


Figure 8. (a) Eigenvalues of the Hessian matrices associated with the horizontal component (circles) and the vertical component (diamonds). (b) Components of the eigenvectors (numbered 1 to 4) associated with the four largest eigenvalues of H_x . The input data include PP reflections for the model in Figure 1 for $X/Z = 2$. The data are contaminated with band-limited (10–25 Hz) random noise; the signal-to-noise ratio is five.

eigenvector associated with the largest eigenvalue of the Hessian points almost entirely in the direction of $V_{hor,P}$ (Figure 5b). As explained above, the amplitude signatures provide additional information for accurate estimation of the parameters V_{P0} , V_{S0} , ϵ , and δ . In particular, errors in the anisotropy coefficients ϵ and δ do not exceed 0.02 (Figure 6).

In the inversion, we assign equal weights to the horizontal and vertical displacement components. For PP-waves recorded on conventional spreads ($X/Z \leq 1.5$), the largest eigenvalues of the Hessian associated with the horizontal component (H_x) are much smaller than those for the vertical component (H_z) (Figure 7). Hence, as expected, the objective function for PP-wave inversion on conventional spreads is more sensitive to the vertical displacement. However, for a longer spread ($X/Z = 2$), the largest eigenvalues of H_x and H_z become comparable (Figure 8a). In addition, the largest eigenvalue of H_x is three times or more the other eigenvalues, and the corresponding eigenvector points in the direction of $V_{hor,P}$ (Figure 8b). Therefore, assigning a larger weight to the horizontal component in the objective function for long spreads may result in a faster convergence toward the velocity $V_{hor,P}$.

Model 2

Next, we test the algorithm on PP and PS data for a stratified model that includes two VTI layers (Figure 9). Again, the parameters of the top (isotropic) layer are fixed at the correct values, and the bottom half-space is known to be isotropic. As was the case for the first model, convergence of the joint PP/PS inversion toward the correct interval parameters is strongly dependent on the initial parameters. If the initial value of δ is set to zero in each layer (which causes a maximum error in δ of just 0.1), the inversion of PP and PS data gets trapped in local minima.

The sensitivity of the inversion to the initial model can be reduced by using a multiscale approach (Bunks et al., 1995). We apply four high-cut filters (limited by 3, 7, 11, and 15 Hz) to the recorded and

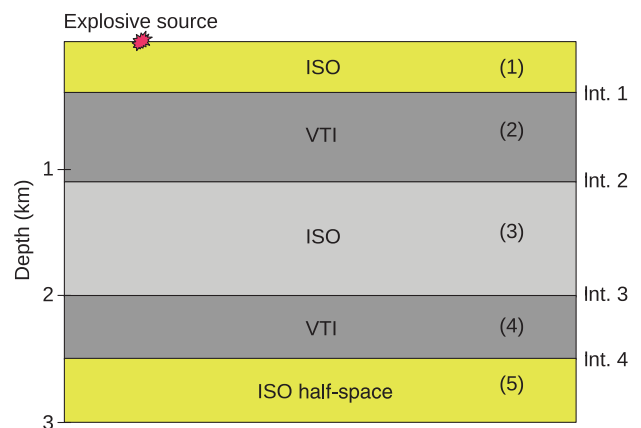


Figure 9. Model with two VTI layers sandwiched between isotropic media. The parameters of layer 1 are $V_P = 2800$ m/s, $V_S = 1400$ m/s, and $\rho = 1.8$ g/cm³; for layer 2, $V_{P0} = 3000$ m/s, $V_{S0} = 1632$ m/s, $\epsilon = 0.1$, $\delta = -0.05$, and $\rho = 2.1$ g/cm³; for layer 3, $V_P = 3400$ m/s, $V_S = 1800$ m/s, and $\rho = 2.4$ g/cm³; for layer 4, $V_{P0} = 3700$ m/s, $V_{S0} = 2000$ m/s, $\epsilon = 0.25$, $\delta = 0.1$, and $\rho = 2.8$ g/cm³; and for the bottom half-space, $V_P = 4300$ m/s, $V_S = 2200$ m/s, and $\rho = 3.1$ gm/cm³.

modeled data and run four iterations for each frequency range. The low frequencies used in the beginning ensure that the objective function has fewer local minima, which are far apart. Therefore, after each update, the solution moves closer to the global minimum. As a result, the algorithm operating with PP and PS data recorded

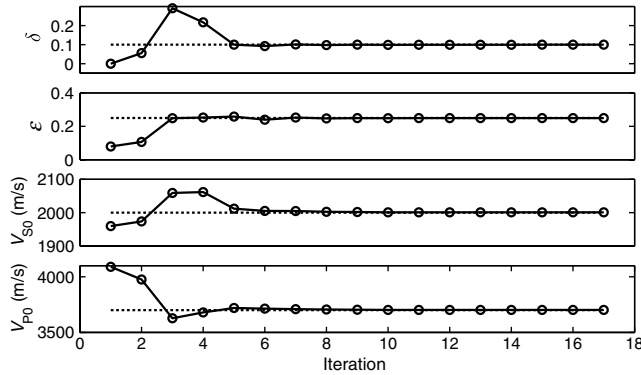


Figure 10. Parameters of layer 4 from the model in Figure 9 after each iteration when inversion is performed using a multiscale approach. The input data include PP and PS reflections; the spreadlength-to-depth ratio for the bottom of the model $X/Z_4 = 1$.

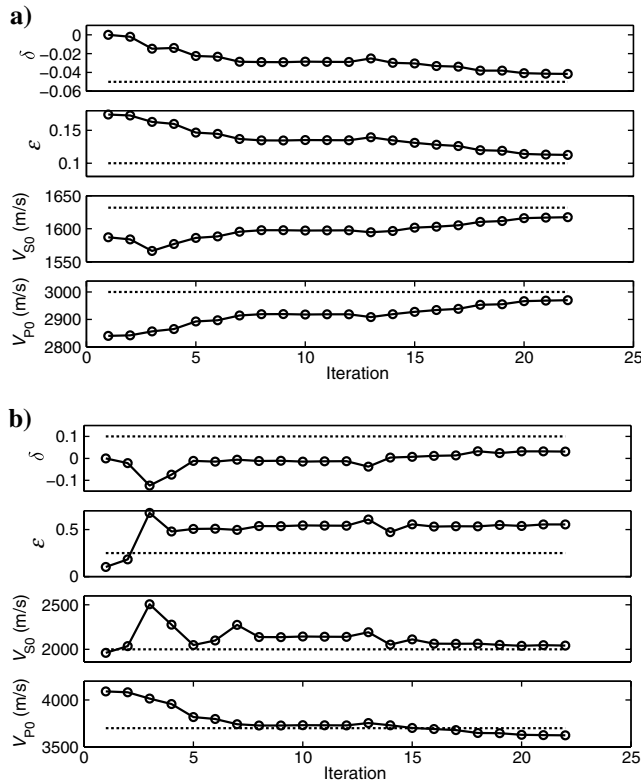


Figure 11. Parameters of (a) layer 2 and (b) layer 4 from the model in Figure 9 after each iteration. The input data include PP reflections; the spreadlength-to-depth ratio for the bottom of layer 2 is $X/Z_2 = 2.2$ (for the bottom of the model, $X/Z_4 = 2$). The data are contaminated with band-limited (10–25 Hz) random noise; the signal-to-noise ratio is 14.

for $X/Z_4 = 1$ (Z_4 is the depth of the bottom of the model) converges from the initial $\delta = 0$ to the correct values in just a few iterations (Figure 10).

When only PP data are inverted, the objective function apparently has a simpler shape (as for the first model), and the multiscale approach proved to be unnecessary. In the remaining tests, we focus on PP-wave inversion and contaminate the input traces with band-limited (10–25 Hz) random noise, as before. The eigenvector/eigenvalue decomposition of the Hessian matrix indicates that the objective function is most sensitive to the parameters V_{P0} , $V_{hor,P}$, and D of the shallow VTI layer and to the P-wave velocity in the isotropic layer immediately below it. The influence of the parameters of the deeper layers on the objective function is much weaker.

If the maximum offset is equal to the depth of the bottom of the model, the spreadlength-to-depth ratio for the bottom of the shallow VTI layer (X/Z_2) is close to 2.2. Then the parameters of that layer are well constrained (Figure 11a), but there are significant errors in ϵ and δ for the deeper VTI layer (Figure 11b). As demonstrated above, inversion for such spreadlengths becomes stable with the addition of PS data (Figure 10).

However, for $X/Z_4 = 2$, the parameters of both VTI layers are accurately resolved with just PP-waves. Even in the presence of moderate band-limited random noise, the velocity V_{P0} for the deeper VTI layer is distorted by less than 2.2%, and the errors in ϵ and δ do not exceed 0.03 (Figure 12b). Therefore, when data

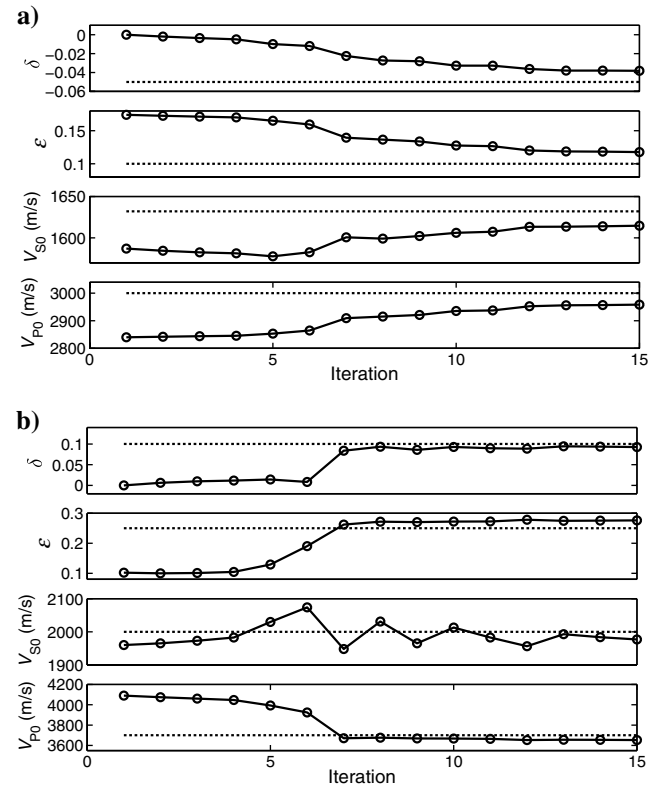


Figure 12. Parameters of (a) layer 2 and (b) layer 4 from the model in Figure 9 after each iteration. The input data include PP reflections; the spreadlength-to-depth ratios are $X/Z_2 \approx 4.5$ and $X/Z_4 = 2$. The data are contaminated with band-limited (10–25 Hz) random noise; the signal-to-noise ratio is 14.

include sufficiently long offsets, it is possible to invert for V_{P0} , V_{S0} , ϵ , and δ with only PP reflections.

CONCLUSIONS

It is well known that the depth scale of horizontally layered VTI models is not constrained by reflection traveltimes of PP- and PS (PSV)-waves, even if long-spread data are acquired. Here, we show that the P- and S-wave interval vertical velocities and anisotropy parameters ϵ and δ of layer-cake VTI media can be estimated by full-waveform inversion of reflection data.

Our gradient-based inversion algorithm operates in the time domain with either PP reflections or the combination of PP-waves and mode-converted PS-waves. Modeling is carried out with the anisotropic reflectivity method, which generates exact 3D multi-component wavefields for laterally homogeneous anisotropic media. The initial model for FWI is obtained from nonhyperbolic moveout inversion followed by kinematic layer stripping. It should be emphasized that our FWI algorithm estimates the parameters of all layers simultaneously to mitigate downward error propagation.

The parameters of the first layer have to be fixed at the correct values. Indeed, the near-surface velocity field on land often is strongly heterogeneous and its influence can be removed using static and datum corrections. Inverting for density increases the nonlinearity of the objective function and creates multiple local minima. Therefore, similar to most published FWI algorithms, we assume density to be known a priori.

First, we examined the inversion for a single VTI layer sandwiched between isotropic media. If the densities are known, the parameters V_{P0} , V_{S0} , ϵ , and δ are well constrained by PP-waves alone. Interestingly, PP data produce accurate parameter estimates even for conventional spreadlengths limited by the reflector depth ($X/Z = 1$) due to additional constraints provided by the reflection coefficient (which is sensitive to V_{S0}) and geometric-spreading factor.

Application of FWI to multilayered VTI models showed that the sensitivity of the objective function to the interval parameters decreases with depth. However, if the ratio X/Z for the bottom of the deepest VTI layer reaches two, its parameters can be obtained from the inversion of PP reflections. Stable parameter estimation for smaller spreads requires the inclusion of PS-waves.

Whereas combining PP data with PS reflections adds useful constraints, it also increases sensitivity to the choice of the initial model. We found that such sensitivity can be mitigated using a multiscale approach, which also improves the convergence of the algorithm.

The wavefields analyzed here are generated for a stack of homogeneous layers and, therefore, do not include diving waves. In practice, diving waves help constrain the low-wavenumber component of the model, whereas reflections improve the spatial resolution. We plan to include diving waves and reflected waves in our FWI algorithm for laterally heterogeneous VTI media, which is currently under development.

The FWI method for stratified VTI media can be generalized for vertical symmetry planes of azimuthally anisotropic models (e.g., orthorhombic). However, geometric spreading in the symmetry planes of orthorhombic media is influenced by azimuthal velocity variations and has to be modeled in 3D.

The developed algorithm should be applicable to many onshore reservoirs, such as unconventional shale plays, which are embedded

in horizontally layered sediments. Our inversion technique based on the Gauss-Newton method cannot be directly extended to laterally heterogeneous media. Still, the presented results provide useful insights for designing inversion operators capable of handling more complicated heterogeneous structures.

ACKNOWLEDGMENTS

We are grateful to the members of the A(nisotropy)-Team of the Center for Wave Phenomena (CWP), Colorado School of Mines (CSM), for fruitful discussions. We would also like to thank J. Behura (CWP) for numerous helpful suggestions. The reviews by the anonymous referees of *GEOPHYSICS* were instrumental in improving the clarity of the manuscript. This work was supported by the Consortium Project on Seismic Inverse Methods for Complex Structures at CWP and by the CIMMM Project of the Unconventional Natural Gas Institute at CSM.

REFERENCES

- Alkhalifah, T., and I. Tsvankin, 1995, Velocity analysis for transversely isotropic media: *Geophysics*, **60**, 1550–1566, doi: [10.1190/1.1443888](https://doi.org/10.1190/1.1443888).
- Bunks, C., F. M. Saleck, S. Zaleski, and G. Chavent, 1995, Multiscale seismic waveform inversion: *Geophysics*, **60**, 1457–1473, doi: [10.1190/1.1443880](https://doi.org/10.1190/1.1443880).
- Chang, H., and G. McMechan, 2009, 3D 3-C full-wavefield elastic inversion for estimating anisotropic parameters: A feasibility study with synthetic data: *Geophysics*, **74**, no. 6, WCC159–WCC175, doi: [10.1190/1.3204766](https://doi.org/10.1190/1.3204766).
- Fryer, G. J., and L. N. Frazer, 1984, Seismic waves in stratified anisotropic media: *Geophysical Journal of the Royal Astronomical Society*, **78**, 691–710, doi: [10.1111/j.1365-246X.1984.tb05065.x](https://doi.org/10.1111/j.1365-246X.1984.tb05065.x).
- Gauthier, O., 1986, Two-dimensional nonlinear inversion of seismic waveforms: Numerical results: *Geophysics*, **51**, 1387–1403, doi: [10.1190/1.1442188](https://doi.org/10.1190/1.1442188).
- Gholami, Y., R. Brossier, S. Operto, V. Prieux, A. Ribodetti, and J. Virieux, 2011, Two-dimensional acoustic anisotropic (VTI) full waveform inversion: The Valhall case study: 81st Annual International Meeting, SEG, Expanded Abstracts, 2543–2548.
- Grechka, V., and I. Tsvankin, 1998, Feasibility of nonhyperbolic moveout inversion in transversely isotropic media: *Geophysics*, **63**, 957–969, doi: [10.1190/1.1444407](https://doi.org/10.1190/1.1444407).
- Grechka, V., and I. Tsvankin, 2002, The joint nonhyperbolic moveout inversion of PP and PS data in VTI media: *Geophysics*, **67**, 1929–1932, doi: [10.1190/1.1527093](https://doi.org/10.1190/1.1527093).
- Kolb, P., F. Collino, and P. Lailly, 1986, Pre-stack inversion of a 1-D medium: *Proceedings of the IEEE*, **74**, 498–508, doi: [10.1109/PROC.1986.13490](https://doi.org/10.1109/PROC.1986.13490).
- Lee, H., J. M. Koo, D. Min, B. Kwon, and H. S. Yoo, 2010, Frequency-domain elastic full waveform inversion for VTI media: *Geophysical Journal International*, **183**, 884–904, doi: [10.1111/j.1365-246X.2010.04767.x](https://doi.org/10.1111/j.1365-246X.2010.04767.x).
- Mallik, S., and L. N. Frazer, 1990, Computation of synthetic seismograms for stratified azimuthally anisotropic media: *Journal of Geophysical Research*, **95**, 8513–8526, doi: [10.1029/JB095iB06p08513](https://doi.org/10.1029/JB095iB06p08513).
- Mora, P., 1987, Nonlinear two-dimensional elastic inversion of multioffset seismic data: *Geophysics*, **52**, 1211–1228, doi: [10.1190/1.1442384](https://doi.org/10.1190/1.1442384).
- Padhi, A., and S. Mallik, 2013, Accurate estimation of density from the inversion of multicomponent prestack seismic waveform data using a non-dominated sorting genetic algorithm: *The Leading Edge*, **32**, 94–98, doi: [10.1190/le32010094.1](https://doi.org/10.1190/le32010094.1).
- Plessix, R., and Q. Cao, 2011, A parameterization study for surface seismic full waveform inversion in an acoustic vertical transversely isotropic medium: *Geophysical Journal International*, **185**, 539–556, doi: [10.1111/j.1365-246X.2011.04957.x](https://doi.org/10.1111/j.1365-246X.2011.04957.x).
- Plessix, R.-E., and H. Rynja, 2010, VTI full waveform inversion: A parameterization study with a narrow azimuth streamer data example: 80th Annual International Meeting, SEG, Expanded Abstracts, 962–966.
- Pratt, R. G., 1999, Seismic waveform inversion in the frequency domain, Part 1: Theory and verification in a physical scale model: *Geophysics*, **64**, 888–901, doi: [10.1190/1.1444597](https://doi.org/10.1190/1.1444597).
- Pratt, R. G., and R. M. Shipp, 1999, Seismic waveform inversion in the frequency domain, Part 2: Fault delineation in sediments using crosshole data: *Geophysics*, **64**, 902–914, doi: [10.1190/1.1444598](https://doi.org/10.1190/1.1444598).
- Rüger, A., 1997, P-wave reflection coefficients for transversely isotropic models with vertical and horizontal axis of symmetry: *Geophysics*, **62**, 713–722, doi: [10.1190/1.1444181](https://doi.org/10.1190/1.1444181).

- Rüger, A., 2002, Reflection coefficients and azimuthal AVO analysis in anisotropic media: SEG.
- Seriff, A. J., and K. Sriram, 1991, P-SV reflection moveouts for transversely isotropic media with a vertical symmetry axis: *Geophysics*, **56**, 1271–1274, doi: [10.1190/1.1443148](https://doi.org/10.1190/1.1443148).
- Song, Z., and P. R. Williamson, 1995, Frequency-domain acoustic-wave modeling and inversion of crosshole data; Part I, 2.5-D modeling method: *Geophysics*, **60**, 784–795, doi: [10.1190/1.1443817](https://doi.org/10.1190/1.1443817).
- Song, Z., P. R. Williamson, and R. G. Pratt, 1995, Frequency-domain acoustic-wave modeling and inversion of crosshole data: Part II — Inversion method, synthetic experiments and real-data results: *Geophysics*, **60**, 796–809, doi: [10.1190/1.1443818](https://doi.org/10.1190/1.1443818).
- Tarantola, A., 1984, Inversion of seismic reflection data in the acoustic approximation: *Geophysics*, **49**, 1259–1266, doi: [10.1190/1.1441754](https://doi.org/10.1190/1.1441754).
- Thomsen, L., 1986, Weak elastic anisotropy: *Geophysics*, **51**, 1954–1966, doi: [10.1190/1.1442051](https://doi.org/10.1190/1.1442051).
- Tsvankin, I., 1995, Body-wave radiation patterns and AVO in transversely isotropic media: *Geophysics*, **60**, 1409–1425, doi: [10.1190/1.1443876](https://doi.org/10.1190/1.1443876).
- Tsvankin, I., 2012, Seismic signatures and analysis of reflection data in anisotropic media, 3rd ed.: SEG.
- Tsvankin, I., and L. Thomsen, 1995, Inversion of reflection traveltimes for transverse isotropy: *Geophysics*, **60**, 1095–1107, doi: [10.1190/1.1443838](https://doi.org/10.1190/1.1443838).
- Wang, X., and I. Tsvankin, 2009, Estimation of interval anisotropy parameters using velocity-independent layer stripping: *Geophysics*, **74**, no. 5, WB117–WB127, doi: [10.1190/1.3157462](https://doi.org/10.1190/1.3157462).
- Xu, X., and I. Tsvankin, 2008, Moveout-based geometrical-spreading correction for PS-waves in layered anisotropic media: *Journal of Geophysics and Engineering*, **5**, 195–202, doi: [10.1088/1742-2132/5/2/006](https://doi.org/10.1088/1742-2132/5/2/006).
- Xu, X., I. Tsvankin, and A. Pech, 2005, Geometrical spreading of P-waves in horizontally layered, azimuthally anisotropic media: *Geophysics*, **70**, no. 5, D43–D53, doi: [10.1190/1.2052467](https://doi.org/10.1190/1.2052467).